Thin-Walled Structures 184 (2023) 110521

Contents lists available at ScienceDirect

Thin-Walled Structures

journal homepage: www.elsevier.com/locate/tws

Full length article

A metamaterial plate with magnetorheological elastomers and gradient resonators for tuneable, low-frequency and broadband flexural wave manipulation

Leizhi Wang [a,b], Zhaobo Chen [a,*], Li Cheng [b]

[a] School of Mechatronics Engineering, Harbin Institute of Technology, Harbin 150001, PR China
[b] Department of Mechanical Engineering, The Hong Kong Polytechnic University, Hong Kong, China

ARTICLE INFO

Keywords:
Metamaterial plate
Magnetorheological elastomer
Multiple gradient resonators
Tuneable bandgaps
Local resonances

ABSTRACT

Incorporating magnetorheological elastomers and multiple gradient resonators (MRE–MGRs), a novel metamaterial plate is proposed, which entails low-frequency, broadband and tuneable bandgap features. The proposed MRE-MGR design embeds an adaptive magnetic field adjustment mechanism to alter the elastic modulus of the MRE to modulate the local resonance bandgap frequency and bandwidth. A bandgap prediction model of the metamaterial plate is developed using the plane wave expansion (PWE) method. Integrated into the model through equivalent stiffness terms, the magneto-controlled modulus of the MRE can be estimated using the energy method and magnetic dipole theory. The established model allows for revealing the dispersion relation of the proposed metamaterial plate under various magnetic fields. The predicted tuneable bandgaps, vibration transmission loss and flexural wave modulation of the metamaterial plate are validated through comparisons with finite element simulations. Numerical analyses show the benefit of the gradient resonator design, which alongside the effective MRE tuning, entails broadening low frequency bandgaps at 92 Hz (relative band of 79.3% for the exponential gradient) and 72.7 Hz (relative band of 65.9% for the linear gradient). The mechanisms underpinning the observed bandgap widening phenomenon are analysed and attributed to the combined effects arising from the gradient design of the distributed resonators and the effective tuning of the MRE elastic modulus under magnetic field modulation. The proposed metamaterial plate functionally achieves simultaneous magnetron adjustment of the bandgap frequency and its width, thus holding great promise for applications such as flexural wave guiding as well as vibration and sound radiation control in planar structures.

1. Introduction

Plate structures are common components for mechanical delivery equipment, such as high-speed train carriages, supersonic aircraft skin and various carrier ship maskings, which are widely used in the transportation engineering field. Such a thin plate structure in larger transport equipment often has low frequency and multiple excitation conditions. Therefore, conventional single-frequency dynamic absorbers cannot meet the actual flexural wave vibration attenuation requirements. Metamaterial plates have been researched on flexural wave regulation, including theoretical methods and topological configuration design.

To break the geometry and mass limitation of phononic crystal plates based on the Bragg scattering mechanism, some typical local resonator structures were proposed for achieving low-frequency and broadband characteristics. For example, core–shell, mass-in-mass, cantilever-type resonator mass-in-membrane and hierarchical elements were discussed for their advantages in manipulating flexural waves and vibration suppression in [1]. The Origami [2,3] and Krigami [4] structures were considered as a lattice design serving a model with broad bandgaps in low frequency. Mechanical metamaterials of pentamode and quasi-zero-stiffness features [5] have sufficient supporting capacity to obtain a low-frequency LR bandgap. Moreover, periodic subwavelength Helmholtz resonators can be used for far-field acoustic wave modulation [6]. A local resonance unit of irregular geometry containing a wedge-mass and wedge-rubber were studied in flexural wave propagation and vibration transmission [7]. A metamaterial plate with plate-like resonators was investigated using a finite element method [8]. Band gap tuning in metamaterial plates can also be achieved by designing resonators within the sandwich structure. For example, a sandwich metamaterial plate was presented by incorporating two coupled sub mass-beam resonators [9] for achieving low and wide frequency bandgaps. The dynamic model and the dispersion equation were derived using energy method. The bandgap

* Corresponding author.
E-mail address: chenzb@hit.edu.cn (Z. Chen).

https://doi.org/10.1016/j.tws.2022.110521
Received 24 September 2022; Received in revised form 23 December 2022; Accepted 31 December 2022
Available online xxxx

properties of a metamaterial sandwich plate with a plate-type resonator following a periodic distribution [10] were numerically and experimentally investigated and the transmission spectra were analysed using finite element method. A sandwich metamaterial plate containing a cantilever beam and mass block fixed between the two faceplates [11] was researched in terms of its dispersion characteristics and vibration transmission. To reach a more ideal bandgap effect, resonators with multiple degrees of freedom (DOF) were considered in some periodic structures. The vibration attenuation and the flexural wave propagation in an elastic metamaterial thin plate were investigated. The plate design involved periodic arrays of multiple degrees of freedom local resonators in square and triangular lattices [12]. A metamaterial plate with 3-DOF high-static-low-dynamic-stiffness (HSLDS) resonators, which consist of a linear spring with a negative stiffness mechanism in parallel [13] was researched, and a dynamic model of a metamaterial plate with nonlinear stiffness under external excitations was established. An elastic metamaterial plate appended 2-DOF local resonance unit was developed using a theoretical model [14]. A dispersion model of the metamaterial plate with an integrated 2-DOF mass–spring subsystem was constructed by the extended Hamilton's principle [15]. Furthermore, strongly nonlinear mechanical metamaterial structures were used for achieving vibration suppression of low frequency and broadband due to bridging coupling of nonlinear local resonance bandgaps [16,17]. The microstructural designs of LR-based elastic metamaterial (EMM) plates [18] have been reviewed. Their potential applications in the fields of low-frequency guided wave attenuation. Most LR bandgap studies of different microstructures were developed using a plane wave expansion method to parse flexural wave guides [19,20]. The above researchers discussed the flexural wave modulation and vibration suppression properties of periodic metamaterials with different local resonance configurations.

In addition, there are a number of metamaterial designs that use active smart materials to regulate the bandgaps, including piezoelectric materials [21–27], thermosensitive materials [28–32], magnetorheological materials [33,34] and electrorheological materials. Adaptive metamaterial structures can be designed for realizing tuneable bandgap characteristics, which use external physical field stimuli control. Piezoelectric metamaterials produce tuneable elastic bandgap characteristics under the action of an external electric field. A composite laminate metamaterial plate with macro-fibre composite piezoelectric patches along one direction [35] was also designed, which was characterized to actively modulate the band gap properties using acceleration feedback control strategy. There is temperature-controlled shape-memory alloys or polymers for the control of metamaterial bandgaps, leading to the migration of bandgaps frequencies. In addition, magnetorheological materials (MRM) have potential applications in bandgap adjustment, producing magneto-induced mechanical properties under the action of external magnetic fields. MRMs have significant advantages of continuity, fast response and reversibility. This paper uses magnetorheological elastomers as a means of bandgap regulation. A brief review of research related to magnetorheological property modulation in metamaterial bandgaps is given in the following context.

Smart materials of the magnetorheological (MR) family have been gradually developed for the study of bandgap regulation of periodic metamaterials due to their special magneto-controlled mechanical properties. A periodic impedance layer filled with MR fluid [36] was proposed to investigate the elastic wave propagation and vibration transmissibility. A transfer model with different distributions, including high- and low-impedance layers, was determined. The dispersion relation is obtained by introducing Floquet's approximate solution under the condition of one-dimensional propagation of plane waves [37]. The effect of the magnetorheological fluid viscosity on the unidirectional band gap is discussed. The MR fluid plays a role in the space–time regulation of the one-dimensional acoustic propagation, and the local acoustic velocity depends on the space–time transformation of the magnetic field. Furthermore, a phononic crystal (PC) with a porous MR elastomer was developed considering buckling deformation [38], which can tune both deformation eigenmodes and bandgaps wide through external magnetic field control. Tuneable phononic crystals under an external magnetic field were proposed to contain a porous hyperelastic magnetorheological elastomer [39]. Based on the MRE static predeformation of unidirectional or bidirectional compression, the motion of progressive time-harmonic plane waves as derived. A metamaterial with a 'lattice-resonator' configuration was developed by a novel additive manufacturing process [40], which can tune bandgaps frequencies to achieve wave guidance by utilizing a magnetic field. The shear wave bandgaps of a 2D phononic crystal composed of a lead column and an MR elastomer matrix were investigated using the PWE method [41]. Shear wave bandgaps can be tuned by applying an external noncontact magnetic field as a frequency-selective filter. Phononic crystals with local resonance properties, including two types of square and spherical structures, were designed using magnetorheological elastomers, which were analysed for the elastic wave bandgaps, transmission and vibration modes of the incident elastic wave [42]. A laminated magnetorheological elastomer isolator with a periodic metamaterial structure was designed to achieve a frequency shift, and the mechanism of bandgaps was analysed [43]. Moreover, 2D PC-based MREs were used for vibration isolation of mechanical equipment at medium and high frequencies [44]. The topology optimization of tuneable PCs with MREs was used for regulating bandgap frequencies [45].

The above references discuss the bandgap regulation of periodic metamaterials and MR materials, but the metamaterial bandgaps in these studies still cannot achieve the flexural wave low-frequency and broadband regulation target. There are complex structures and magnetic field sources that are not easy to implement in these studies. Therefore, we develop a novel metamaterial plate with MRE–MGRs including an adaptive magnetic field to address the above problems. In this study, a theoretical magneto-mechanical model was established using a magnetic dipole model via the energy method. A flexural wave bandgap model using both equivalent stiffness and magneto-induced modulus was proposed, which provides a theoretical method for verifying the bandgap regulation of metamaterial plates with MRE–MGRs. The periodic metamaterial plate with MRE–MGRs was discussed with regard to the influence of the magneto-induced mechanical properties of MREs on bandgap frequencies. The effect of the MRE zero-field modulus on the bandgap tuning of the metamaterial plate is analysed. The vibration transmission and bandgap eigenvalue results were evaluated using a 3D finite element model. The metamaterial plate bandgap model was verified by eigenvalue calculation in the finite element method. Furthermore, the magneto-mechanical model of anisotropic MREs was validated by a compressive experiment employing the MTS mechanical machine. Anisotropic MR elastomers of different volume fractions were fabricated by embedding carbonyl iron particles (CIPs) arranged along a perpendicular magnetic chain. The conclusion was that both the gradient design concept and the MRE bandgap frequency of the MRE-MGR metamaterial plate have significant advantages.

2. Design and modelling

2.1. MRE-MGR design

A set of dual-cantilever beams with gradient length is designed to achieve low-frequency and broadband modulation using a series–parallel coupling. These MRE–MGRs can achieve adaptive magnetic modulation without external energy devices, as shown in Fig. 1(a). MRE–MGRs with an MR elastomer are appended on the surface of the substrate plate to achieve magneto-control modulation, mainly including an MR elastomer, magnetic field adjustment device and double cantilever beams. An MR elastomer as a connection between the double cantilever beams and the substrate achieves subsystem stiffness modulation. A magnetic field adjustment device is used to control the magnetic induction of the MRE by changing its height from the bottom.

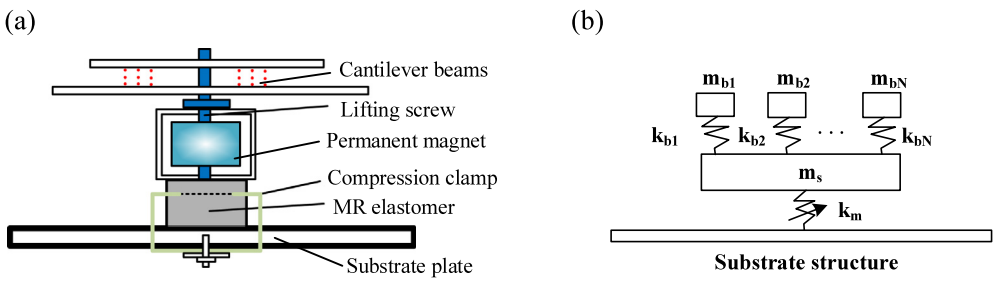

Fig. 1. The structure and principal diagrams: (a) the MRE-MGR unit; (b) the MRE-MGR unit of discrete dynamics.

The double-cantilever beam length has a gradient variation for covering more low-frequency bandgaps. Fig. 1(b) shows the discrete model of the MRE–MGRs, including the two-stage tandem structure, to achieve an overall reduction in the MRE-MGR stiffness.

A gradient design concept is adopted for the length of the cantilever beam in the MRE–MGRs to achieve low frequency and broadband function, as shown in Eq. (1). In this study, we adopt two gradient forms containing a linear gradient and a power exponential gradient, which are used as the gradient design paradigm to discuss the bandgap regulation laws of the metamaterial plate.

$$L_{bi} = L_{bI} + (I - i)\,\Delta L, i = 1, 2, 3, \ldots, I. \tag{1}$$

$$\Delta L = \begin{cases} ab^i, \text{exponential gradient} \\ c, \text{ linear} \end{cases}$$

where ΔL is the length gradient; L_{bI} is the length of the ith double cantilever beam in MRE–MGRs; c is a linear gradient; and ab^i is an exponential gradient. The local resonance bandgaps theory of multiple DOF realizes that the multiple DOF resonators in MRE–MGRs act in parallel at the same position on the substrate plate. Therefore, it is necessary to equivalently transform the discrete model shown in Fig. 1(b) into the discrete parallel resonators model in Fig. 2. The equivalent dynamic equations of the discrete models in Fig. 2 can be expressed as Eq. (2). A flexural wave bandgap theory using equivalent stiffness is proposed for the proposed metamaterial plate in Section 2.2.

$$\begin{gathered} \left(m_s + m_{b1}\right)\ddot{x}_1 + \frac{k_{b1}k_m}{k_{b1}+k_m}x_1 = F\sin(\omega t + \varphi) \\ \vdots \\ \left(m_s + m_{bN}\right)\ddot{x}_N + \frac{k_{bN}k_m}{k_{bN}+k_m}x_N = F\sin(\omega t + \varphi) \end{gathered} \tag{2}$$

$$\begin{bmatrix} k_1 & 0 & 0 & \cdots & 0 \\ 0 & k_2 & 0 & \vdots & \vdots \\ 0 & 0 & k_3 & \vdots & \vdots \\ \vdots & \vdots & \cdots & \ddots & 0 \\ 0 & 0 & \cdots & 0 & k_N \end{bmatrix}$$

$$= \begin{bmatrix} \frac{k_{b1}k_m}{k_m+k_{b1}} & 0 & 0 & \cdots & 0 \\ 0 & \frac{k_{b1}k_m}{k_m+k_{b2}} & 0 & \vdots & \vdots \\ 0 & 0 & \frac{k_{b3}k_m}{k_m+k_{b3}} & \vdots & \vdots \\ \vdots & \vdots & \cdots & \ddots & 0 \\ 0 & 0 & \cdots & 0 & \frac{k_{bN}k_m}{k_m+k_{bN}} \end{bmatrix}$$

$$\begin{bmatrix} m_1 & 0 & 0 & \cdots & 0 \\ 0 & m_2 & 0 & \cdots & 0 \\ 0 & 0 & m_3 & \cdots & 0 \\ \vdots & \cdots & \cdots & \ddots & \vdots \\ 0 & \cdots & \cdots & \cdots & m_{N+1} \end{bmatrix}$$

$$= \begin{bmatrix} m_s + m_{b1} & 0 & 0 & \cdots & 0 \\ 0 & m_s + m_{b2} & 0 & \cdots & 0 \\ 0 & 0 & m_s + m_{b3} & \cdots & 0 \\ 0 & \cdots & \cdots & \ddots & 0 \\ 0 & \cdots & \cdots & 0 & m_s + m_{bN} \end{bmatrix}$$

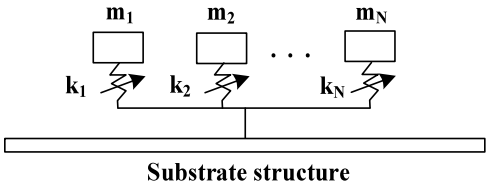

Fig. 2. Equivalent discrete dynamic system of MRE–MGRs..

2.2. Metamaterial plate bandgap model

Based on the plane wave expansion method, the position vector of the single cell of the 2D local resonance metamaterial plate in the x-y plane can be expressed as Eq. (3)

$$R = \overline{m}a_1 + \overline{n}a_2 \tag{3}$$

where m and n are positive integers. From the Kirchhoff plate theory, the dynamic equations of a periodic metamaterial plate with an additional local resonance unit are expressed as Eq. (4).

$$\begin{gathered} D\nabla^4 w(r) - \omega^2 \rho h w(r) = \sum_{i=1}^{N}\sum_{R}\left[f_i(R) + \omega^2 m_{0i} w(R)\right]\delta(r - R) \\ f_i(R) = -k_i\left[w(R) - u_i(R)\right]\; i = 1, 2, \ldots, N \\ -\omega^2 m_i u_i(R) = -f_i(R)\; i = 1, 2, \ldots, N \end{gathered} \tag{4}$$

where $D = Eh^3/12\left(1 - v^2\right)$ is the bending stiffness of the thin plate; E and ρ denote the Young's modulus and density of the thin plate material, respectively; h denotes the thickness of the thin plate; ω is the angular frequency; vector $\boldsymbol{r}$ is the coordinate vector at any point in the 2D plane of the thin plate; $w(r)$ is expressed as the transverse vibration displacement of the thin plate at the r coordinate; $u_i(R)$ is the vibration displacement of mass m_i of the ith metamaterial unit located at R; and $f_i(R)$ is the reaction force of the ith MRE-MGR at the R coordinate for the thin plate. Expanding the 2D δ function in Eq. (4) as $\delta(\vec{r} - \vec{R}) = \delta\left(x - \vec{R}_x\right)\delta\left(y - \vec{R}_y\right)$, the transverse vibrational displacement of the periodic metamaterial plate can be expanded into an infinite order plane wave superposition form $w\left(\vec{r}\right) = \sum_{\vec{G}} W_{\vec{G}} e^{-i(\vec{k}+\vec{G})\vec{r}}$, where $\boldsymbol{k}$ is the Bloch wave vector, $\boldsymbol{W}_{\mathbf{G}}$ is the plane wave amplitude, and $\boldsymbol{G}$ is the inverse grid vector. According to Bloch's theorem, the periodic condition function is obtained as Eq. (6).

$$\begin{aligned} w(\vec{R}) &= w(0)e^{-i\vec{k}\cdot\vec{R}} \\ u_i(\vec{R}) &= u_i(0)\,e^{-i\vec{k}\cdot\vec{R}} \end{aligned} \tag{5}$$

According to the properties of the δ function as Eq. (6), we can obtain Eq. (7)

$$\sum_{R} e^{-i\vec{k}\cdot\vec{R}}\delta\left(\vec{r} - \vec{R}\right) = e^{-i\vec{k}\cdot\vec{r}}\sum_{\vec{R}}\delta\left(\vec{r} - \vec{R}\right) \tag{6}$$

$$D\nabla^4 w(r) - \omega^2 \rho h \omega(r) = \sum_{j=1}^{N} \left\{ [-k_j [w(0) - u_j(0)] + \omega^2 m_{0j} \omega(0)] \times e^{-i\vec{k}\cdot\vec{r}} \sum_R \delta(\vec{r} - \vec{R}) \right\}$$
$$-\omega^2 m_j u_j(0) = k_j \left[w(0) - u_j(0) \right] \tag{7}$$

The infinite summation δ function on the right-hand side of the equation can be treated as a periodic function, which is expanded into Fourier series form $\sum_{\vec{R}} \delta\left(\vec{r} - \vec{R}\right) = \sum_{\vec{G}} e^{-i\vec{G}\cdot\vec{r}}/S$.

$S = \left|a_1 \times a_2\right|$ is expressed as the area of the metamaterial unit. The periodic metamaterial plate bandgap theory using the PWE method obtains the dynamic equations expressed as Eqs. (8) and (9).

$$DS|k+G|^4 W_G + \sum_{j=1}^{N}(k_j \sum_G W_G) - \sum_{j=1}^{N} k_j u_j - \omega^2 \rho h S W_G - \omega^2 \sum_{j=1}^{N} \left(m_{0j} \sum_G W_{G'} \right) = 0 \tag{8}$$

$$-\omega^2 m_j u_j = k_j \left(\sum_{G'} W_{G'} - u_j \right) \tag{9}$$

where u_j is jth MRE-MGR displacement; m_j is jth MRE-MGR mass. To solve the periodic metamaterial plate bandgap model, the infinite order truncation treatment is taken as a finite order PWE. The plane wave order used in the calculation is $\overline{M} = (2M+1)^2$. Eqs. (8) and (9) can be written in simplified form as Eq. (10).

$$\left([K] - \omega^2 [M] \right) \{W\} = 0 \tag{10}$$

Thus, the stiffness matrix K and the mass matrix M in the flexural wave bandgap model using equivalent stiffness are expressed as Eqs. (11) and (12), respectively.

$$[K] = \begin{bmatrix} DS[K_G] + \sum_{j=1}^{N} k_j [U_j] & -\frac{k_{b1}k_m}{k_m+k_{b1}}[Q] & -\frac{k_{b1}k_m}{k_m+k_{b2}}[Q] & \cdots & -\frac{k_{bN}k_m}{k_m+k_{bN}}[Q] \\ -\frac{k_{b1}k_m}{k_m+k_{b1}}[Q'] & \frac{k_{b1}k_m}{k_m+k_{b1}} & 0 & \cdots & 0 \\ -\frac{k_{b1}k_m}{k_m+k_{b2}}[Q'] & 0 & \frac{k_{b1}k_m}{k_m+k_{b2}} & \vdots & \vdots \\ \vdots & \vdots & \cdots & \ddots & 0 \\ -\frac{k_{bN}k_m}{k_m+k_{bN}}[Q'] & 0 & \cdots & 0 & \frac{k_{bN}k_m}{k_m+k_{bN}} \end{bmatrix} \tag{11}$$

$$[M] = \begin{bmatrix} \rho h S[I] + \sum_{j=1}^{N} m_{0j} [U_j] & 0 & 0 & \cdots & 0 \\ 0 & m_s + m_{b1} & 0 & \cdots & 0 \\ 0 & 0 & m_s + m_{b2} & \vdots & \vdots \\ \vdots & \vdots & \cdots & \ddots & 0 \\ 0 & 0 & \cdots & 0 & m_s + m_{bN} \end{bmatrix} \tag{12}$$

$$[K_G] = \begin{bmatrix} |k+G_1|^4 & 0 & \cdots & 0 \\ 0 & |k+G_2|^4 & \cdots & \vdots \\ \vdots & \vdots & \ddots & 0 \\ 0 & \cdots & 0 & |k+G_{\overline{M}}|^4 \end{bmatrix} [Q] = \begin{bmatrix} 1 \\ 1 \\ \vdots \\ 1 \end{bmatrix}_{\overline{M}+1}$$

$$[Q'] = [Q]^T \quad [I] = \begin{bmatrix} 1 & 0 & \cdots & 0 \\ 0 & 1 & \cdots & \vdots \\ \vdots & \vdots & \ddots & 0 \\ 0 & \cdots & 0 & 1 \end{bmatrix}_{\overline{M}\times\overline{M}}$$
$$[U] = [QQ']^T$$

$$[W] = \begin{Vmatrix} W_G \\ u_1 \\ u_2 \\ \vdots \\ u_N \end{Vmatrix} \quad [W_G] = \begin{Vmatrix} W_{G_1} \\ W_{G_2} \\ \vdots \\ W_{G_M} \end{Vmatrix}$$

2.3. MREs magneto-induced mechanical model

The energy method is used to derive a magneto-induced mechanical model for anisotropic magnetorheological elastomers considering preload deformation. The modulation of the bandgap frequency of the proposed metamaterial plate depends on the magnetic energy density function $\boldsymbol{W_m}$ of the MR elastomer, which affects the magneto-induced modulus. Therefore, according to Rosensweig's theory [46], the interaction energy $E_{i,j+1}$ between two magnetic dipoles in the MRE matrix is calculated as shown in Eq. (13).

$$E_{i,i+1} = \frac{1}{4\pi\mu_0\mu_l} \left[\frac{\vec{m}_i \cdot \vec{m}_{i+1}}{r^3} - \frac{3}{r^5} \left(\vec{m}_i \cdot \vec{r}\right) \left(\vec{m}_{i+1} \cdot \vec{r}\right) \right] \tag{13}$$

where r is the distance between magnetic dipoles and i and $i+1$ are adjacent magnetic dipoles. m_i is the magnetic dipole moment of the ith magnetic dipole under an external magnetic field in Eq. (14).

$$\vec{m}_i = \frac{4}{3}\pi a^3 \mu_0 \mu_l \chi H_i \tag{14}$$

where H_i is the magnetic flux density of the particle; χ is the specific magnetization of the particle; a is the diameter of the particle; and μ_l and μ_0 are the relative magnetic permeability of the magnetic particle and silicone rubber, respectively. The magnetic field of magnetic dipole i is influenced not only by the applied magnetic field H_0 but also by the magnetic field generated by the magnetic particles around magnetic dipole i in the same chain. Therefore, the composite magnetic flux density considering the magnetization of magnetic particles can be obtained for magnetic dipole i.

$$H_i = \vec{H}_0 + 2\sum_{j=1}^{n} \frac{3\vec{r}\left(\vec{r}_j \cdot \vec{m}_j\right) - \vec{m}_j}{4\pi\mu_0\mu_l r_j^3} \tag{15}$$

where $\boldsymbol{m_j}$ is the magnetic dipole moment of magnetic particle j. $\boldsymbol{r_j}$ is the distance between magnetic particles i and j, which is the unit vector in its direction. When considering only the interaction between magnetic particles in a single chain, assume that the distance between each pair of adjacent particles is equal. r denotes the average distance between two particles, so $\boldsymbol{r_j} = j\boldsymbol{r}$. Assume that each particle has the same magnetic dipole moment; then $\boldsymbol{m_i} = \boldsymbol{m_j} = \boldsymbol{m}$. The magnetic dipole moment of magnetic particle i can be obtained by combining Eqs. (14) and (15).

$$\vec{m} = \frac{4}{3}\pi a^3 \mu_0 \mu_l \chi H_0 \left[\frac{1}{1 - (4/3)\chi\xi (a/r)^3} \right] \tag{16}$$

where $\xi = \sum_{\infty}^{j=1} \frac{1}{j^3} \approx 1.202$; $r = r_0(1+\varepsilon)$; ε is the compression strain. The whole magnetic energy in MR elastomers is expressed as Eq. (17).

$$E_s = \frac{\varphi V}{4/3\pi a^3} \cdot \frac{2\xi |m|^2}{4\pi\mu_0\mu_l r^3} \tag{17}$$

Thus, the magnetic energy density function is expressed as Eq. (18).

$$W_m = \frac{E_s}{V} = \frac{1}{\left[r_0^3(1+\varepsilon)^3 - \frac{4}{3}\chi\xi a^3\right]\left[1 - \frac{4}{3}\chi\xi\frac{a^3}{r_0^3(1+\varepsilon)^3}\right]} \tag{18}$$

The distribution of the magnetic field causes a significant change in the mechanical properties of the MR elastomer. The magneto-induced modulus is indicated as a physical equation with both magnetic material and strain parameters, as shown in Eq. (19).

$$E_m = \Delta E = \frac{\partial^2 W_m}{\partial \varepsilon^2} = p\frac{6q^2(\varepsilon+1) + 36q(\varepsilon+1)^4 + 12(\varepsilon+1)^7}{\left[q - (\varepsilon+1)^3\right]^4} \tag{19}$$
$$p = \frac{3\varphi\xi}{8\pi^2 a^3 \mu_0 \mu_l r_0^3} \left(\frac{4}{3}\pi a^3 \mu_0 \mu_l \chi \overline{H}_0\right)^2$$
$$q = \frac{4}{3}\chi\xi\frac{a^3}{r_0^3}$$

Table 1
Calculation parameters of the theoretical model.

Parameter		Symbol	Reference values
Magnetic chain microstructure	Diameter of the particle	a	3–8 μm
	Reduced spacing of adjacent magnetic dipoles	r_0/a	1.8
Material magnetic properties	Matrix permeability	μ_1	1
	Vacuum permeability	μ_0	$4\pi \times 10^{-7}$ T m/A
	Specific magnetization of the CIPs	χ	0.65
Carbonyl iron powder volume fraction		φ	60/80%
Compression strain		ε	0–20%

The magneto-induced stiffness of the link between the MRE–MGRs and the substrate plate in the metamaterial plate can be expressed as

$$k_m = \frac{E_{sum}A}{h} = \frac{A}{h}\left(E_0 + p\frac{6q^2(\varepsilon+1) + 36q(\varepsilon+1)^4 + 12(\varepsilon+1)^7}{\left[q-(\varepsilon+1)^3\right]^4}\right) \tag{20}$$

where E_{sum} is the MRE compressive elastic modulus and E_0 is the initial modulus under zero-field conditions.

3. Results and discussions

MR elastomers are used as the MRE–MGRs of the metamaterial plate to realize contact stiffness modulation between the element and substrate plate. The magneto-mechanical properties of an anisotropic MR elastomer are proposed to achieve a large MR effect considering compressive strain. The compressive magneto-induced modulus is derived using magnetic dipole theory to analyse the regulation of the bandgap frequency of the metamaterial plate. In the designed MRE–MGRs, the height adjustment of the permanent magnet is used to control the MRE magnetic field. The MRE elastic modulus changes by a large amount with the magnetic field strength, which affects the contact stiffness between the MRE–MGRs and the substrate plate. Based on the magneto-induced constitution model of the MR elastomer, the magnetic parameters and the microstructure parameters shown in Table 1 are used to analyse the influence of magnetic flux density and compression deformation on the magneto-induced modulus.

3.1. Validation of bandgap theory using equivalent stiffness

The Kirchhoff plate theories can be used as simplification terms for modelling flexural wave propagation in metamaterial plates. However, this treatment might be misleading in the case of wave modes that can rise on a 3D (3D) FEM model. Thus, it might be interesting to compute bandgaps using 3D geometric modelling to assess wave modes in the dispersion relations to determine whether these will affect the flexural wave propagation characteristics of the substrate plate. The proposed metamaterial plate is different from the traditional periodic local resonance plate to achieve bandgap adjustment. The anisotropic MREs are employed as the stiffness regulation function, and are connected with the double cantilever beams of the gradient design parameters. The double cantilever beam resonators use the fundamental frequency of the vibration mode to achieve the bandgaps of the metamaterial plate.

A metamaterial plate with B1–B1 is employed as a general case to validate the bandgap model using equivalent stiffness. Frequency dispersion curves of the metamaterial plate with B1–B1 beams include multiple horizontal dispersion of A1–A8 wave modes, as shown in Fig. 3(a). Compared to the results of the bandgap model using equivalent stiffness in Fig. 3(b), the curved parts of the flexural wave dispersion have a similar trend. The vibration transmission loss in the attenuation regions of the finite metamaterial plate was investigated, as shown in Fig. 3(c). This shows that the local resonance bandgap frequency is consistent with the bandgap position of both the 3D FEM model and the theoretical bandgap model. To illustrate the A1–A8 wave modes, the eigenmodes of the periodic metamaterial plate are analysed in Fig. 3(d). The modal deformation of the double cantilever beams (modes A1, A3, A5, A7, and A8), in terms of the transverse displacement along the z-direction which is perpendicular to the plane of the metamaterial plate, is shown by colour bars. However, these modes have different vibration shapes in cantilever beams, and the A7 and A8 modes have small vibrations in the MRE oscillator. The A2 wave mode in the vicinity of the first local resonance bandgap occurs when cantilever beams flip along the width direction. Furthermore, the computed bandgaps in the A4 and A6 modes depend on the rotational mode, which demonstrates rotational shape displacements in the x-y plane of both the cantilever beams and MRE oscillator. The above eigenmodes have a common feature in which the flexural wave cannot propagate on the substrate plate, which illustrates that the A1–A8 modes for the flexural wave bandgaps are invalid modes.

The 3D models of the 10 × 10 finite metamaterial plate corresponding to the case (power exponential gradient) are modelled using meshes made of hexahedral solid elements with 76,955 nodes. These 3D models can be used to obtain the assembled mass and stiffness matrix using trilinear isoparametric shape functions with full Gauss quadrature integration. This FE model of a metamaterial plate computes bandgaps using a wave finite element (WFE) method as proposed by Mace and Manconi [47,48], restricting the periodicity and the wave vector to the x-y plane. The objective is to assess whether there are differences between wave modes obtained both using FEM with 3D geometry and the PWE method. The boundary conditions of the metamaterial plate are free on all four sides of the plate, and displacement excitation is used to act at the edge midpoint (yellow point) of the metamaterial plate. The results extract the velocity transmission response of the finite period metamaterial plate at the start and end frequencies of the bandgap, as shown in Fig. 4. The flexural waves along the x and y directions are significantly attenuated, which verifies the accuracy of the dispersion relation using the equivalent stiffness.

3.2. The effect of magnetic field modulation on the LR bandgap

3.2.1. Adaptive magnetic field distribution

The adaptive magnetic field device is used in the metamaterial plate to achieve vertical magnetic field regulation without an external electromagnetic source. The permanent magnet is mounted on the lifting frame such that the vertical adjustment range is 8 mm, as shown in Fig. 1(a). The magnetic field distribution of different height positions can be obtained using Maxwell FEM package simulation. The magnetic field strength of the area below the device is significantly enhanced as the height of the permanent magnet decreases, as shown in Fig. 5(a)(b)(c). The device generates a flux density that gradually decreases along the MRE thickness direction, as indicated in Fig. 5(d). The midpoint position corresponding to the magnetic flux density can be regarded as the magnetic parameter of bandgap modulation according to the MR elastomer thickness dimension. The simulation results show that the maximum magnetic flux density is 320 mT.

3.2.2. Bandgap manipulation

The external magnetic field parameter is adjusted by the height of the permanent magnet in the MRE–MGRs. The anisotropic MR elastomer is used as the magnetic control stiffness function in the metamaterial plate, as shown in Fig. 1. The MR elastomer shape parameters are set to 10 × 10× 5 mm in length, width and thickness. The shape of the permanent magnet is a hollow cylinder 20 × 20 mm in diameter and height, which has a mass of 0.075 kg. These MRE–MGRs lead to a magneto-induced modulus modulation that eventually changes the mechanical dynamics of the metamaterial plate. In addition, double cantilever beam resonators with gradient designs in MRE–MGRs were investigated using PWE bandgap theory with equivalent stiffness. The double cantilever beam resonators of a specific gradient design are shown in Table A.2 and A.3.

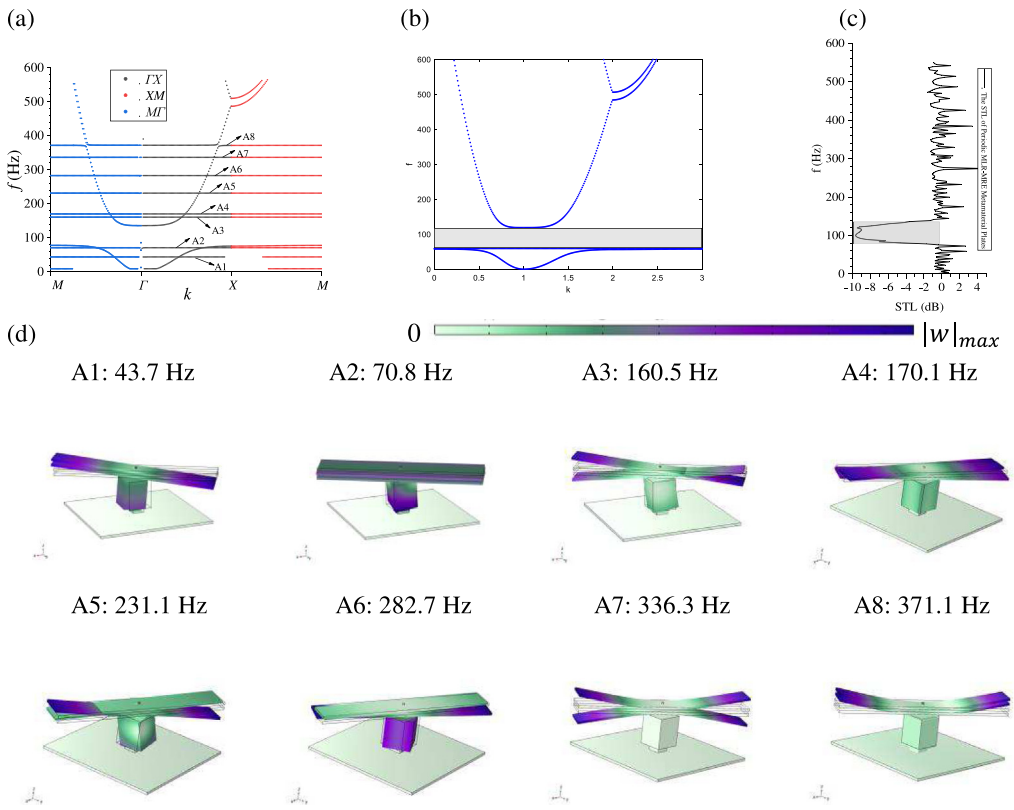

Fig. 3. (a) Dispersion curve of the metamaterial plate with B1–B1 beams from the FEM model (b) dispersion curve of the metamaterial plate by bandgap theory using equivalent stiffness. (c) vibration transmission loss of the finite metamaterial plate with B1–B1 beams. (d) A1–A8 mode shapes corresponding to displacement fields.

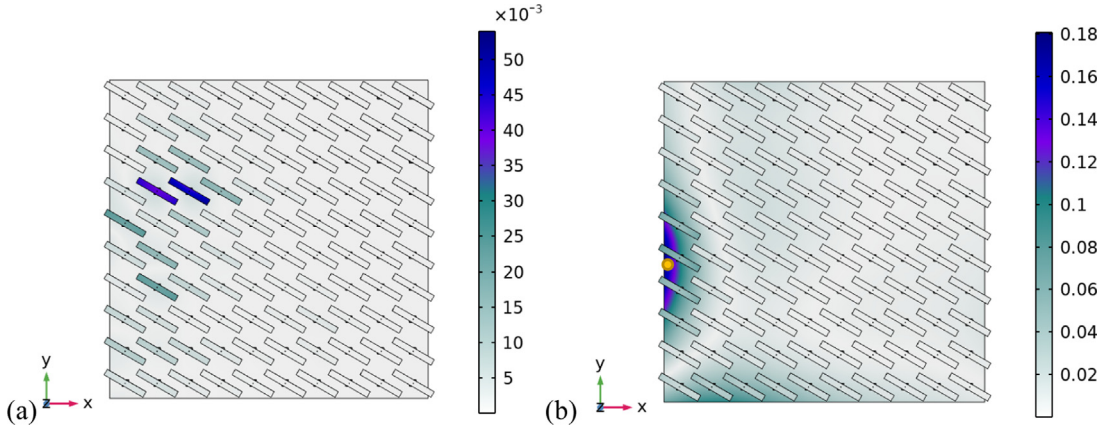

Fig. 4. The velocity field of the metamaterial plate (B1–B1 beams): (a) frequency response of the starting local resonance bandgap (78.2 Hz); (b) frequency response of the cut-off local resonance bandgap (138.9 Hz) (m/s). (For interpretation of the references to colour in this figure legend, the reader is referred to the web version of this article.)

The MRE–MGRs are discretized to obtain the dynamic mechanical model shown in Fig. 1(b). The dynamic mechanical results were numerically simulated to analyse the fundamental frequency of the MRE–MGRs. The frequency components of the MRE–MGRs of the power exponential gradient are distributed around four main frequencies of 330, 420, 540 and 738 Hz, as shown in Fig. 6(b). However, the MRE–MGRs of the linear gradient are concentrated at approximately 500 Hz, as shown in Fig. 6(a). This evidence also confirms that the gradient design concept is more conducive to opening the local resonance bandgaps of the metamaterial plate.

The zero-field initial modulus of MR elastomers is sensitive to the dynamic characteristics of MRE–MGRs. The effect of the MRE initial modulus on the dispersion relation is studied by PWE bandgap theory using equivalent stiffness. The dispersion curves of both the linear gradient and power exponential gradient design corresponding to the first to third local resonance bandgaps of the metamaterial plate are broadened using the modulation of the zero-field initial modulus, as shown in Fig. 7(a)(b)(c)(d). The fourth bandgap corresponding to the metamaterial plate of the power exponential gradient represents an increasing and then decreasing trend. However, the fourth bandgap of the metamaterial plate with a linear gradient increases as the zero-field initial modulus increases. The metamaterial plate of the power exponential gradient design has a larger broad bandgap region than the linear gradient design due to the power exponential gradient involving a more scattered fundamental frequency distribution. The comparison shows that two types of gradient designs are more beneficial to

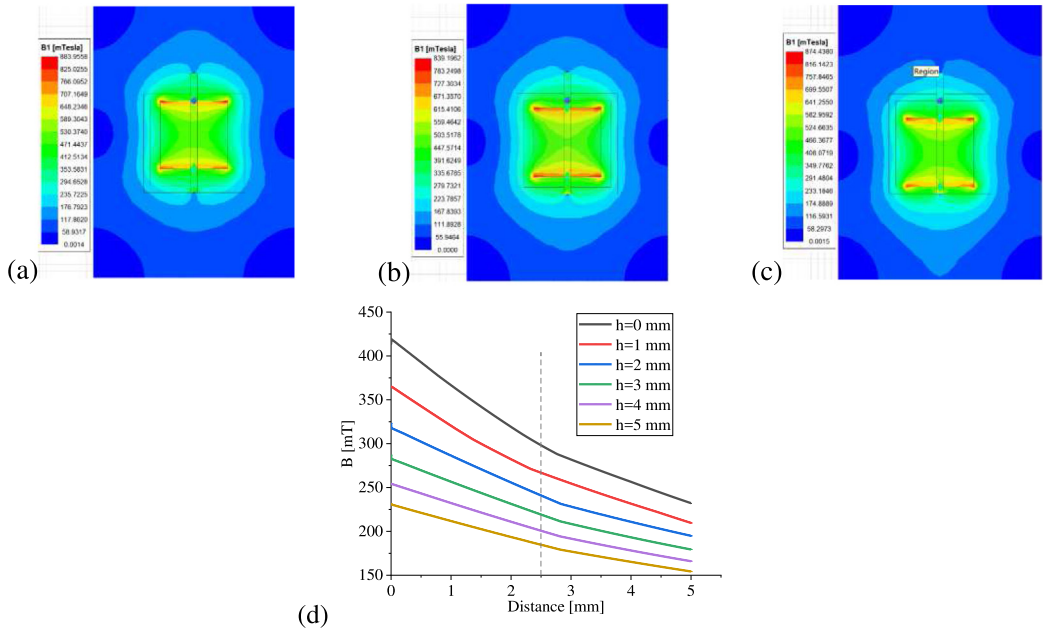

Fig. 5. The magnetic field distribution generated by the adaptive device at different heights: (a) height = 5 mm, (b) height = 2 mm, (c) height = 0 mm, and (d) magnetic flux density along the MRE thickness.

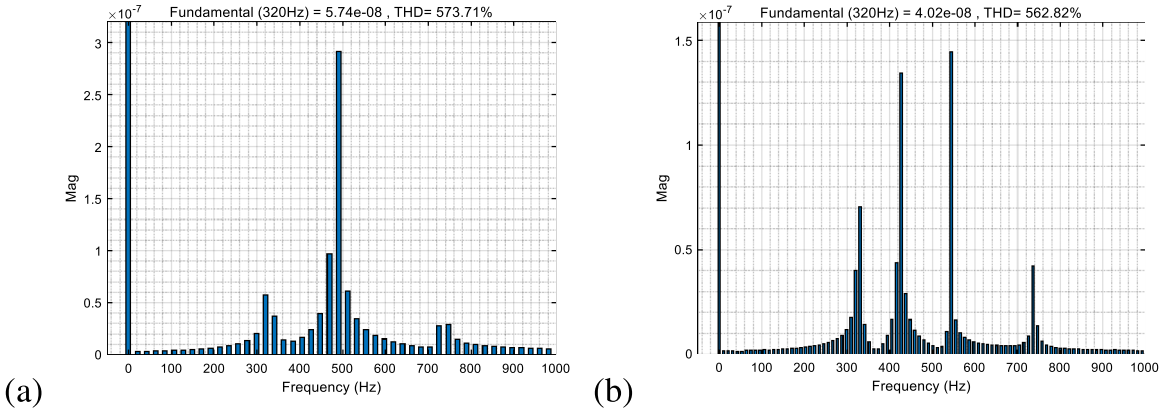

Fig. 6. Frequency component analysis of MRE–MGRs: (a) linear gradient; (b) power exponential gradient.

open broadband-based local resonance mechanisms. The advantage of the gradient design method is that the metamaterial plate forms a multifrequency broadband to achieve vibration reduction and flexural wave suppression. The gradient design method overcomes the narrow bandgap defect of traditional local resonance periodic plates.

In addition, the dispersion curves of the metamaterial plate with a power exponential gradient exhibit a warping phenomenon at the wave vector Γ that expands the MΓ directional (45°) bandgap width as the zero-field modulus of MR elastomers gradually increases. The wave vector X is the immobile point with respect to the dispersion curves of the metamaterial plate of the linear gradient design in Fig. 7(c)(d). Thus, the above conclusions show that the zero-field modulus of MR elastomers has a significant effect on the bandgap width of periodic metamaterial plates.

The bandgap regulation capability of the proposed metamaterial plate with the gradient design under a magnetic field was investigated using PWE bandgap theory with equivalent stiffness. The results show that the metamaterial plate with a power exponential gradient is more conducive to enhancing the fourth LR bandgap under magnetic field modulation, as shown in Fig. 8(a)(b). The bandgap openings of the metamaterial plate with gradient design are observed through the MR elastomer elastic modulus under magnetic field modulation. When the adaptive magnetic field modulation is increased to the maximum, the fourth LR bandgap cut-off frequency of the metamaterial plate of the power exponential gradient reaches 290 Hz, while the cut-off frequency of the linear gradient is 266 Hz. The proposed metamaterial bandgaps of magnetic field modulation can reach a switch function as flexural wave propagation. Although the bandgaps have moved up, the first three orders of magnitude of the local resonance bandgaps are slightly opened. The first three local resonance bands slightly increase from 7.1 Hz to 28.1 Hz and from 8 Hz to 31.1 Hz in the metamaterial plate with resonants structure with linear gradient and exponential gradient, respectively. The fourth resonance band gap is widened by 50 Hz such that the relative bandwidth reaches 78.3%. Although the starting frequency of the fourth bandgap increases to 61.1 Hz, the bandwidth grows from 101.9 Hz to 157.6 Hz in the structure with

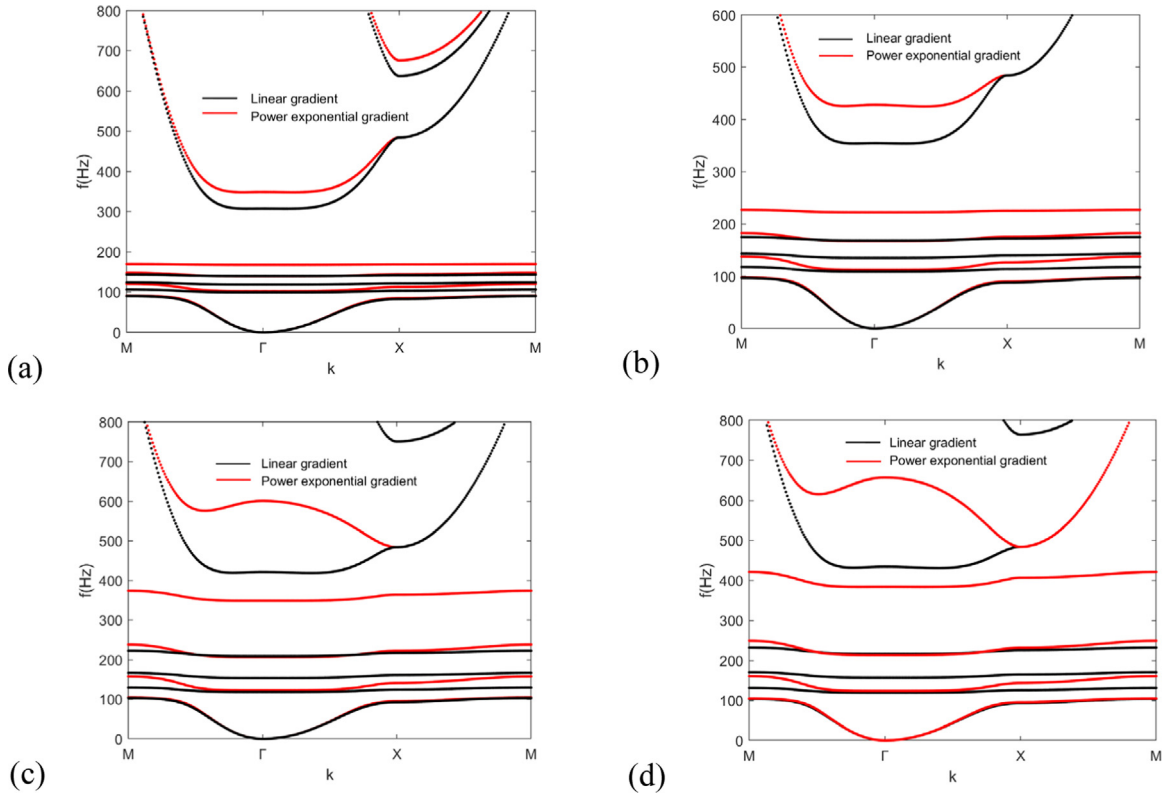

Fig. 7. The effect of the zero-field modulus on the bandgap of the metamaterial plate with a double-cantilever beam length gradient design: (a) $E_0 = 5 \times 10^6$ Pa; (b) $E_0 = 1 \times 10^7$ Pa; (c) $E_0 = 5 \times 10^7$ Pa; (d) $E_0 = 1 \times 10^8$ Pa.

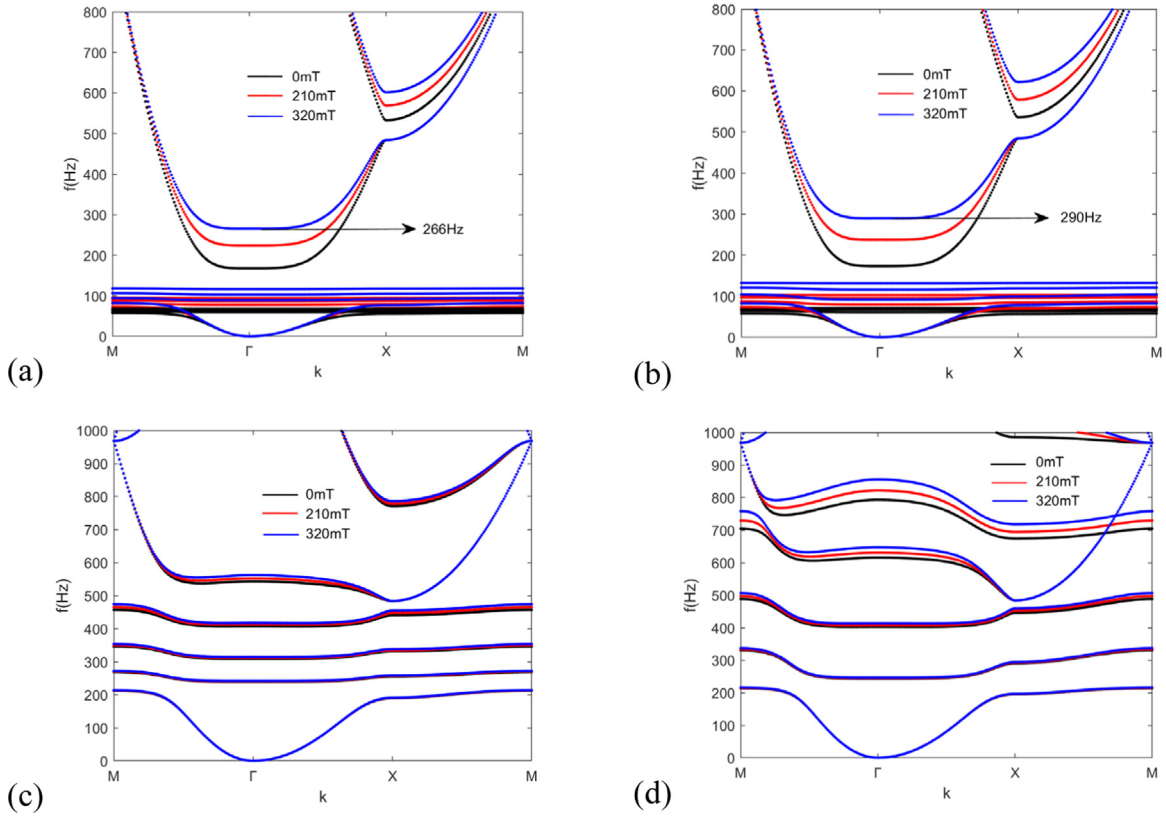

Fig. 8. The influence of magnetic flux density on the bandgap regulation of the metamaterial plate: (a) linear gradient ($E_0 = 8 \times 10^5$ Pa, $\varepsilon = 0.1$); (b) power exponential gradient ($E_0 = 8 \times 10^5$ Pa, $\varepsilon = 0.1$); (c) linear gradient ($E_0 = 2 \times 10^7$ Pa, $\varepsilon = 0.15$); (d) power exponential gradient ($E_0 = 2 \times 10^7$ Pa, $\varepsilon = 0.15$).

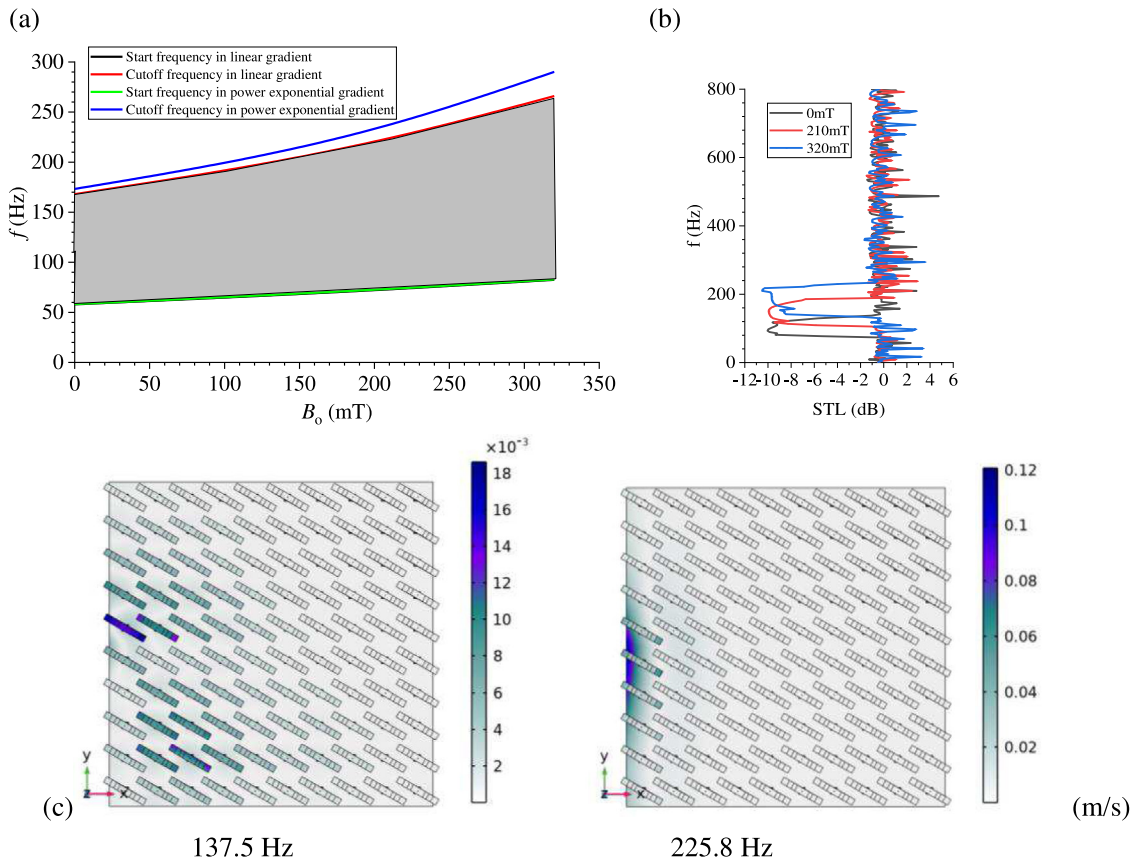

Fig. 9. (a) Bandgap modulation of the metamaterial plate of linear and power exponential gradients; (b) influence of magnetic flux density on vibration velocity transmission loss in a power exponential gradient ($E_0 = 8 \times 10^5$ Pa, $\varepsilon = 0.1$); (c) vibration velocity field of the finite metamaterial plate with a power exponential gradient at start (left) and cut-off (right) frequencies.

exponential gradient resonators. Moreover, the first three local resonance bandwidths all open gradually as the magnetic field increases. As a result, the expansion of the first three bands compensates for the deterioration of the low-frequency region due to the shifted fourth band. The mechanical properties of the magnetoelastic material and the geometric parameters of the double cantilever beam resonators significantly affect the band gap features. The starting frequency of the low-frequency region is controlled by the resonators' mass. In any event, the design mechanism proposed in this paper allows for possible tuning of the band gaps. Since the mass of the adaptive magnetic field device is larger than that of the cantilever beam resonators, the bandgap adjustment of the magnetic field is mainly focused on the cut-off frequency of the fourth LR bandgap.

When the adaptive magnetic field device mass limitation is not considered, the variation law of bandgap dispersion is studied using a smaller oscillator mass of 0.01 kg. The dispersion curves also undergo warping at the cut-off frequency of the fourth LR band gap in the x-direction in Fig. 8(c)(d). The metamaterial plate with a linear gradient has a small change in the band width under magnetic field modulation, in contrast to the metamaterial plate with a power exponential gradient, which has an obvious ability to modulate bands. In conclusion, the reasonable matching of the MRE-MGR mass and the zero-field mechanical properties of the MRE should be considered using an optimization tool to utilize the ideal magnetron adjustment capability of the bandgaps of the metamaterial plate.

The gradient design method in bandgap regulation with advantages is performed referencing linear gradient and power exponential gradient to assess the presence of attenuation regions associated with bandgaps. In addition, it should be noted that the other types of gradient designs in the metamaterial plate have similar advantages on low frequency and broadbands.

The dispersion characteristics of the metamaterial plate under magnetic field modulation are investigated using the PWE bandgap model with the equivalent stiffness. The bandgap regulation ability of a metamaterial plate with a power exponential gradient of a 3D structure is further evaluated using the finite element method, as shown in Fig. 9(a). The metamaterial plate of power exponential gradient and linear gradient exhibit that the lower edge of the bandgap remains stable, while the cut-off frequency of upper edge becomes fast growth with the increase of magnetic flux density. The comparison results indicate that the growth rate of the LR bandgap of the power exponential gradient is faster. The bandgap width presents a small difference corresponding to the two types of metamaterial plates when the attenuation region of the zero-field condition (110.2 Hz for the linear gradient and 116 Hz for the power exponential gradient). In addition, the bandgap width is extended when the flux density reaches 320 mT, which realizes a relative band 105.4% (182.9 Hz) of the linear gradient design and relative band 111.9% (208.6 Hz) of the power exponential gradient design considering magnetic modulation ability. This suggests that gradient design can achieve the extended attenuation regions promoting magnetic modulation.

The results reveal that the flexural wave transmission loss of the metamaterial plate under the magnetic field mainly reflects the attenuation ability of the LR bandgaps, as shown in Fig. 9(b). Since the influence of the first to third bandgaps is relatively weak, the transmission characteristics of the finite metamaterial plate present an

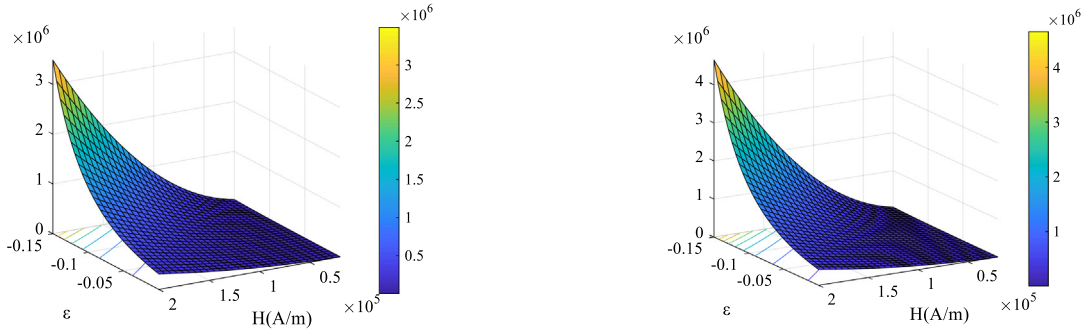

(a) 60% Carbonyl iron powder volume fraction (b) 80% Carbonyl iron powder volume fraction

Fig. A.1. The anisotropic MRE magneto-induced modulus of different volume fractions with increasing magnetic flux density and compressive strain.

entire attenuation region. The velocity vibration response field at a magnetic field strength of 320 mT has an attenuated bandgap centre frequency of approximately 180 Hz, which is in basic agreement with the bandgap theory results. The vibration velocity field response of the metamaterial plate with a power exponential gradient at the start and cut-off frequencies (320 mT), as shown in Fig. 9(c) suggests that the flexural waves are significantly suppressed in the 2D direction. The observation on the left side of Fig. 9(c) shows that the lower start frequency of the bandgap of the gradient design resonators results in stronger synergistic coupling than the cut-off frequency to achieve low-frequency flexural wave vibration reduction performance.

4. Conclusion

This paper proposes an innovative metamaterial plate with an adaptive magnetic field source that enhances the multifrequency coupling effect and broadens the low-frequency bandgaps. Two types of designs of linear gradient and power exponential gradient are used as paradigms for study, demonstrating that the concept of gradient design for the metamaterial plate is more conducive to bandgap widening and magnetron regulation. A PWE bandgap model using equivalent stiffness is established, which provides a theoretical method for studying the bandgap regulation of the metamaterial plate.

Low bandgap regulation can be realized by developing a metamaterial plate with different gradient functions. In addition, the dispersion curve of the metamaterial plate with exponential power undergoes a warping phenomenon in the fourth LR bandgap as the MRE elastic modulus increases. This phenomenon suggests the directional broadband of the fourth local resonance. The flexural wave modulation of a 2D periodic metamaterial plate was presented using PWE and FEM methods. The metamaterial plate of gradient design provides a large design space for low frequency bandgaps, including both double cantilever beams with gradient and magneto-controlled MRE, which demonstrate significant application potential in flexural wave modulation and vibration suppression. Low-frequency vibration suppression and flexural wave manipulation in thin plate structures are important topics attracting the widespread attention from both scientific and engineering community. In this sense, the metamaterial plate incorporating tunable MRE properties offer an attractive alternative to the existing design reported in the literature. Through effective wave manipulation, problems like vibration energy insulation inside structural assembly, structural sound radiation control or directional transmission/modulation of waves can be potentially tackled.

CRediT authorship contribution statement

Leizhi Wang: Software, Methodology, Investigation, Formal analysis, Conceptualization. **Zhaobo Chen:** Supervision. **Li Cheng:** Writing – review & editing, Supervision, Methodology.

Declaration of competing interest

The authors declare the following financial interests/personal relationships which may be considered as potential competing interests: CHEN Zhaobo reports financial support was provided by Harbin Institute of Technology. CHENG Li reports financial support was provided by The Hong Kong Polytechnic University.

Data availability

No data was used for the research described in the article.

Acknowledgements

Financial support from the National Key R&D Program of China (2019YFE0116200) and Central Research Grant (CRG) of Hong Kong PolyU and supervision and revision support from Prof. Li Cheng and Prof. Zhaobo Chen are gratefully acknowledged.

Appendix

The compressive strain can be used to enhance the MR effect to improve the stiffness regulation capability of the MRE–MGRs. A comparison of the results in Fig. A.1 shows that the precompression deformation strategy is beneficial to enhance the regulation of MRE stiffness and overcome the limitations of this adaptive magnetic field regulation.

Experimental assessment of magneto-induced modulus

MR elastomers play the role of stiffness regulation in the proposed metamaterial plate. The magneto-induced modulus under compressive strain is deduced from the magnetic dipole theory, which reveals the nonlinear mechanical properties. This shows that the magnetic flux density has a quadratic relationship with the magneto-induced modulus, while the compressive strain has a more complex polynomial exponential relationship. The magneto-induced modulus of different volume fractions containing carbonyl iron particles (CIPs) can be analysed using the magneto-induced mechanical theoretical model, as shown in Fig. A.1(a)(b). Anisotropic MR elastomers with 20 × 20× 10 mm rectangular blocks of 60% and 80% mass fraction CIPs were prepared in the same way as in the literature [49]. Soft CIPs of 10 μm diameter were selected for mixing into a silicone rubber matrix. The precursor was defoamed in a −0.1 MPa pressure environment for 10 min. Finally, the precursor was vulcanized under 0.8 T vertical magnetic field and room temperature. The anisotropic MRE samples were tested on an MTS mechanical experimental machine equipped with a custom-designed magnetic coil compression fixture. The hysteresis curves of

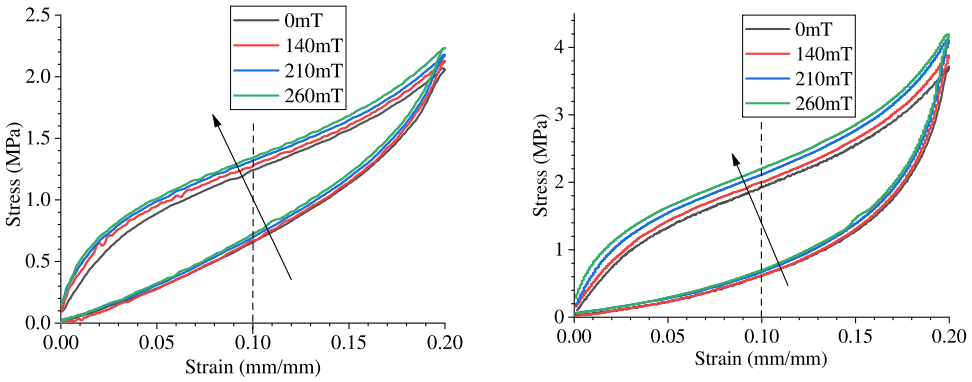

Fig. A.2. The MRE stress–strain curve of magneto-induced compressive strain (a) 60% mass fraction; (b) 80% mass fraction.

Table A.1
The relations of the magneto-induced modulus under compressive strain $\varepsilon = 0.1$.

PRM	60% mass fraction			80% mass fraction		
B_o	140 mT	210 mT	260 mT	140 mT	210 mT	260 mT
Exp. E_m (Pa)	3.30×10^5	7.80×10^5	1.18×10^6	5.20×10^5	1.28×10^6	1.86×10^6
Theory E_m (Pa)	3.57×10^5	8.03×10^5	1.23×10^6	5.05×10^5	1.14×10^6	1.74×10^6
Error	8.18%	2.95%	4.24%	2.88%	10.93%	6.45%

Table A.2
The double cantilever beam parameters of linear length variation ($\Delta L = 0.02$).

Parameter	L (m)	t (m)	w (m)	$2l_r$ (m)	m_0 (kg)	m_r (kg)	k_b (N/m)	f_r (Hz)
B1	0.14	0.002	0.02	0.138	0.0061	0.0090	42483.3	345.5
B2	0.12	0.002	0.02	0.118	0.0052	0.0077	67953.1	472.5
B3	0.1	0.002	0.02	0.098	0.0044	0.0064	118625.2	685.0
B4	0.08	0.002	0.02	0.078	0.0035	0.0051	235272.6	1081.4

Table A.3
The double cantilever beam parameters of nonlinear length variation ($\Delta L = 0.05 * 0.8^i$).

Parameter	L (m)	t (m)	w (m)	$2l_r$ (m)	m_0 (kg)	m_r (kg)	k_b (N/m)	f_r (Hz)
B1	0.14	0.002	0.02	0.138	0.0061	0.0090	42483.3	345.5
B2	0.1	0.002	0.02	0.098	0.0044	0.0064	118625	685
B3	0.068	0.002	0.02	0.066	0.003	0.0043	388350	1510.4
B4	0.042	0.002	0.02	0.0404	0.00194	0.0026	1693210.7	4031.1

compressive strain–stress at different magnetic flux densities were obtained as shown in Fig. A.2. The magneto-induced modulus of 60% and 80% mass fraction MREs at 0.1 strain were analysed from the experimental results. The compressive test results compared with the theoretical results of the magneto-induced mechanical model are shown in Table A.1. The maximum error was 10.93%, and the minimum error was 2.88%. The reasons have both mechanical machine testing errors and magnetic field inhomogeneities provided by the compression coil fixture.

The OAT (one-at-a-time) method is used to analyse the sensitivity of the geometric parameters of the resonators in the metamaterial plate model. These parameters vary to cover different ranges, but with the same variation amplitude. The OAT ignores the interconnections between parameters and allows the identification of more sensitive ones. A relative sensitivity (RS) index is defined as

$$RS = \left| \frac{[y(x + \Delta x) - y(x)]/y(x)}{\Delta x / x} \right|$$

where x denotes the value of a targeted geometric parameter; Δx is its variation (0.02 m); $y(x)$ and $y(x+\Delta x)$ represent the model output before and after the change of the parameter respectively. A larger RS value indicates a higher sensitivity of the parameter to affect the band gap and vice versa. Using the definition, a sensitivity analysis on band gap is carried out on the geometric parameters of the double cantilever beam resonators including its length L, width w and thickness t within a reasonable variation range. Fig. A.3 below shows the effect of the

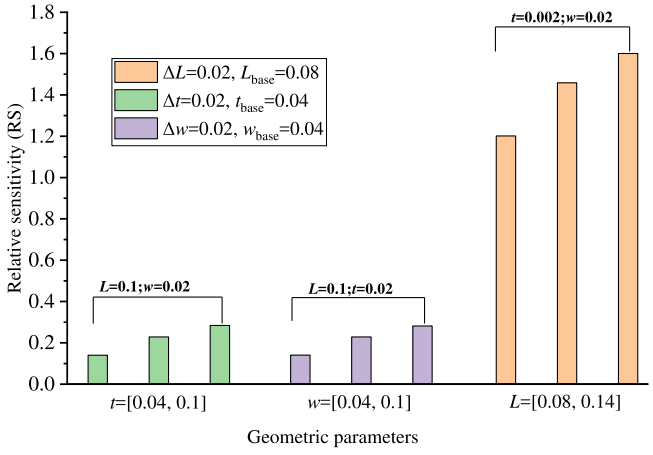

Fig. A.3. Sensitivity analysis of geometric parameters of the double cantilever beam resonator on the band gap (Incremental intervals of the parameters are ΔL, Δt, and Δw, respectively; baseline values are denoted by L_{base}, t_{base}, and w_{base}, respectively).

geometrical parameters on the band gap in the MRE-regulated metastructure with a single resonator utilizing relative sensitivity. When L varying between 0.08–0.14 m with a step size $\Delta L = 0.02$ m, it shows much higher relative sensitivity (maximum value of 1.6) than the width

w and thickness t. The incremental intervals for the width and thickness are $\Delta t = 0.02$ m and $\Delta w = 0.02$ m, respectively.

References

[1] L. Wu, Y. Wang, K. Chuang, F. Wu, Q. Wang, W. Lin, H. Jiang, A brief review of dynamic mechanical metamaterials for mechanical energy manipulation, Mater. Today 44 (2021) 168–193.

[2] S. Sadeghi, S. Li, Harnessing the quasi-zero stiffness from fluidic origami for low frequency vibration isolation, in: Smart Materials, Adaptive Structures and Intelligent Systems, American Society of Mechanical Engineers, 2017, V002T03A008.

[3] D. Zhang, B. Ji, X. Zhou, A numerical study of the dynamic properties of Miura folded metamaterials, Aerosp. Syst. 2 (2) (2019) 125–135.

[4] R. Zhu, H. Yasuda, G.L. Huang, J.K. Yang, Kirigami-based elastic metamaterials with anisotropic mass density for subwavelength flexural wave control, Sci. Rep. 8 (1) (2018) 483.

[5] K. Wang, J. Zhou, D. Tan, Z. Li, Q. Lin, D. Xu, A brief review of metamaterials for opening low-frequency band gaps, Appl. Math. Mech. 43 (7) (2022) 1125–1144.

[6] F. Lemoult, M. Fink, G. Lerosey, Acoustic resonators for far-field control of sound on a subwavelength scale, Phys. Rev. Lett. 107 (6) (2011) 064301.

[7] K. Lu, G. Zhou, N. Gao, L. Li, H. Lei, M. Yu, Flexural vibration bandgaps of the multiple local resonance elastic metamaterial plates with irregular resonators, Appl. Acoust. 159 (2020).

[8] J. Jung, S. Goo, S. Wang, Investigation of flexural wave band gaps in a locally resonant metamaterial with plate-like resonators, Wave Motion 93 (2020).

[9] X. Fan, J. Li, X. Zhang, F. Li, Multi-bandgaps metamaterial plate design using complex mass-beam resonator, Int. J. Mech. Sci. 236 (2022).

[10] Q. Wang, J. Li, Y. Zhang, Y. Xue, F. Li, Bandgap properties in metamaterial sandwich plate with periodically embedded plate-type resonators, Mech. Syst. Signal Process. 151 (2021).

[11] J. Li, X. Fan, F. Li, Numerical and experimental study of a sandwich-like metamaterial plate for vibration suppression, Compos. Struct. 238 (2020).

[12] E.J.P. Miranda, E.D. Nobrega, A.H.R. Ferreira, J.M.C. Dos Santos, Flexural wave band gaps in a multi-resonator elastic metamaterial plate using Kirchhoff–Love theory, Mech. Syst. Signal Process. 116 (2019) 480–504.

[13] K. Wang, J. Zhou, C. Cai, D. Xu, H. Ouyang, Mathematical modeling and analysis of a meta-plate for very low-frequency band gap, Appl. Math. Model. 73 (2019) 581–597.

[14] K. Lu, J.H. Wu, L. Jing, N. Gao, D. Guan, The two-degree-of-freedom local resonance elastic metamaterial plate with broadband low-frequency bandgaps, J. Phys. D: Appl. Phys. 50 (9) (2017).

[15] H. Peng, P. Frank Pai, H. Deng, Acoustic multi-stopband metamaterial plates design for broadband elastic wave absorption and vibration suppression, Int. J. Mech. Sci. 103 (2015) 104–114.

[16] X. Fang, J. Wen, B. Bonello, J. Yin, D. Yu, Ultra-low and ultra-broad-band nonlinear acoustic metamaterials, Nature Commun. 8 (1) (2017) 1–11.

[17] P. Sheng, X. Fang, J. Wen, D. Yu, Vibration properties and optimized design of a nonlinear acoustic metamaterial beam, J. Sound Vib. 492 (2021) 115739.

[18] R. Zhu, X.N. Liu, G.K. Hu, F.G. Yuan, G.L. Huang, Microstructural designs of plate-type elastic metamaterial and their potential applications: a review, Int. J. Smart Nano Mater. 6 (1) (2015) 14–40.

[19] V.F. Dal Poggetto, A.L. Serpa, Flexural wave band gaps in a ternary periodic metamaterial plate using the plane wave expansion method, J. Sound Vib. 495 (2021).

[20] A.F. Russillo, G. Failla, A novel reduced-order dynamic-stiffness formulation for locally resonant metamaterial plates, Compos. Struct. 280 (2022).

[21] M.A. Nouh, O.J. Aldraihem, A. Baz, Periodic metamaterial plates with smart tunable local resonators, J. Intell. Mater. Syst. Struct. 27 (13) (2016) 1829–1845.

[22] N. Kherraz, L. Haumesser, F. Levassort, P. Benard, B. Morvan, Hybridization bandgap induced by an electrical resonance in piezoelectric metamaterial plates, J. Appl. Phys. 123 (9) (2018).

[23] R.L. Thomes, J.A. Mosquera-Sánchez, C. De Marqui, Bandgap widening by optimized disorder in one-dimensional locally resonant piezoelectric metamaterials, J. Sound Vib. 512 (2021).

[24] C. Sugino, M. Ruzzene, A. Erturk, An analytical framework for locally resonant piezoelectric metamaterial plates, Int. J. Solids Struct. 182–183 (2020) 281–294.

[25] C. Sugino, M. Ruzzene, A. Erturk, Merging mechanical and electromechanical bandgaps in locally resonant metamaterials and metastructures, J. Mech. Phys. Solids 116 (2018) 323–333.

[26] Y. Liu, H. Wang, W. Fang, Q. Han, D. Liu, Y. Liang, Tunable control of subwavelength topological interface modes in locally resonance piezoelectric metamaterials, Compos. Struct. 276 (2021).

[27] C. Sugino, S. Leadenham, M. Ruzzene, A. Erturk, An investigation of electroelastic bandgap formation in locally resonant piezoelectric metastructures, Smart Mater. Struct. 26 (5) (2017).

[28] C. Nimmagadda, K.H. Matlack, Thermally tunable band gaps in architected metamaterial structures, J. Sound Vib. 439 (2019) 29–42.

[29] Z. Chen, G. Wang, Y. Mao, C.W. Lim, New metamaterial mathematical modeling of acoustic topological insulators via tunable underwater local resonance, Appl. Math. Model. 108 (2022) 258–274.

[30] S. Yang, X. Zhou, Y.-F. Wang, Tunable band gap and wave guiding in periodic grid structures with thermal sensitive materials, Compos. Struct. 290 (2022).

[31] J.-X. Wang, X. Liu, Q.-S. Yang, R. Tao, Y. Li, L.-H. Ma, A novel programmable composite metamaterial with tunable Poisson's ratio and bandgap based on multi-stable switching, Compos. Sci. Technol. 219 (2022).

[32] R. Noroozi, M. Bodaghi, H. Jafari, A. Zolfagharian, M. Fotouhi, Shape-adaptive metastructures with Variable Bandgap Regions by 4D printing, Polymers (Basel) 12 (3) (2020).

[33] W. Yan, G. Zhang, Y. Gao, Investigation on the tunability of the band structure of two-dimensional magnetorheological elastomers phononic crystals plate, J. Magn. Magn. Mater. 544 (2022).

[34] L. Shaogang, Y. Zhao, D. Zhao, J. Wu, C. Gao, Tunable elastic wave bandgaps and waveguides by acoustic metamaterials with magnetorheological elastomer, Acoust. Phys. 66 (2) (2020) 123–131.

[35] T. Ren, F. Li, Y. Chen, C. Liu, C. Zhang, Improvement of the band-gap characteristics of active composite laminate metamaterial plates, Compos. Struct. 254 (2020).

[36] D. Zhao, X. Shi, S. Liu, F. Wang, Theoretical and experimental investigation on wave propagation in the periodic impedance layered structure modulated by magnetorheological fluid, J. Intell. Mater. Syst. Struct. 31 (6) (2020) 882–896.

[37] A. Nanda, M.A. Karami, One-way sound propagation via spatio-temporal modulation of magnetorheological fluid, J. Acoust. Soc. Am. 144 (1) (2018) 412.

[38] A. Bayat, F. Gordaninejad, Dynamic response of a tunable phononic crystal under applied mechanical and magnetic loadings, Smart Mater. Struct. 24 (6) (2015).

[39] A. Bayat, F. Gordaninejad, Band-gap of a soft magnetorheological phononic crystal, J. Vib. Acoust. 137 (1) (2015).

[40] C.D. Pierce, C.L. Willey, V.W. Chen, J.O. Hardin, J.D. Berrigan, A.T. Juhl, K.H. Matlack, Adaptive elastic metastructures from magneto-active elastomers, Smart Mater. Struct. 29 (6) (2020).

[41] Z. Xu, F. Wu, Z. Guo, Shear-wave band gaps tuned in two-dimensional phononic crystals with magnetorheological material, Solid State Commun. 154 (2013) 43–45.

[42] Z. Xu, J. Tong, F. Wu, Magnetorheological elastomer vibration isolation of tunable three-dimensional locally resonant acoustic metamaterial, Solid State Commun. 271 (2018) 51–55.

[43] Z. Chen, S. Sun, L. Deng, J. Yang, S. Zhang, H. Du, W. Li, Investigation of a new metamaterial magnetorheological elastomer isolator with tunable vibration bandgaps, Mech. Syst. Signal Process. 170 (2022).

[44] G.-J. Yu, X.-X. Wen, C.-B. Du, L.-Y. Wang, S.-J. Zhu, Study on bandgap vibration isolation of super-cell phononic crystals based on magnetorheological elastomers, AIP Adv. 11 (12) (2021).

[45] Liang, Kuan, et al., Topology optimization of magnetorheological smart materials included PnCs for tunable wide bandgap design, Acta Mech. Sinica 38 (3) (2022) 1–13.

[46] R.W. Chantrell, Ferrohydrodynamics: R.E. Rosensweig, Cambridge University Press, Cambridge, ISBN: 0521 25624 0, 1985, p. 344, 45.00, hardback. Phys. Earth Planetary Interiors 46 (1987) 389-390.

[47] B.R. Mace, E. Manconi, Modelling wave propagation in two-dimensional structures using finite element analysis, J. Sound Vib. 318 (4) (2008) 884–902.

[48] V.F.D. Poggetto, A.L. Serpa, Elastic wave band gaps in a three-dimensional periodic metamaterial using the plane wave expansion method, Int. J. Mech. Sci. 184 (2020) 105841.

[49] H. Vatandoost, M. Hemmatian, R. Sedaghati, S. Rakheja, Dynamic characterization of isotropic and anisotropic magnetorheological elastomers in the oscillatory squeeze mode superimposed on large static pre-strain, Composites B 182 (2020).